CORA Cork Open Research Archive
Cartlann Taighde Oscailte Chorcaí

Title	DeltaFlex—An additively manufactured Delta robot with compliant joints: Virtual prototyping and experimental evaluation
Authors	Parmiggiani, Alberto;Ottonello, Emilio;Kargar, Seyyed Masoud;Baggetta, Mario;Hao, Guangbo;Berselli, Giovanni
Publication date	2024-07-22
Original Citation	Parmiggiani, A., Ottonello, E., Kargar, S. M., Baggetta, M., Hao, G., and Berselli, G. (2024) 'DeltaFlex—An additively manufactured Delta robot with compliant joints: Virtual prototyping and experimental evaluation', Journal of Mechanisms and Robotics, 16(11), 111011(10pp). https://doi.org/10.1115/1.4065780
Type of publication	Article (peer-reviewed)
Link to publisher's version	10.1115/1.4065780
Rights	© 2024, ASME. This Accepted Manuscript is available for reuse under a Creative Commons Attribution (CC BY 4.0) licence: https://creativecommons.org/licenses/by/4.0/ - https://creativecommons.org/licenses/by/4.0/
Download date	2026-11-13 05:53:59
Item downloaded from	https://hdl.handle.net/10468/16183

UCC
University College Cork, Ireland
Coláiste na hOllscoile Corcaigh

DeltaFlex - an Additively Manufactured Delta Robot with Compliant Joints: *Virtual Prototyping and Experimental Evaluation*

Alberto Parmiggiani, Emilio Ottonello, Seyyed Masoud Kargar, Mario Baggetta, Guangbo Hao, Giovanni Berselli

***Abstract*—The current study presents the development and validation of a compliant Delta robot with a monolithic structure, which has been fabricated using additive manufacturing (AM). The monolithic design and the use of AM accelerate the robot development cycle by enabling rapid prototyping and deployment while also facilitating experimentation with novel or different robot kinematics. The use of flexible joints for robots presents a challenge in achieving sufficient workspaces. However, parallel architectures are well-suited for incorporating compliant joints, as they require lower ranges of motion for individual joints compared to serial architectures. Therefore, the Delta configuration has been chosen for this study. Multi-body Flexible Dynamics (MfBD) simulations have been used as a means to guide design choices and simulate the structural behaviour of the robot. A Design for Additive Manufacturing (DfAM) technique has been adopted to minimize the need for support structures and maximize mechanical strength. The quantitative evaluation of the Delta's overall performance has been conducted in terms of stiffness and precision. The stiffness test aimed to gauge the robot's ability to withstand applied loads, whereas the repeatability test assessed its precision and accuracy. This approach offers a promising path for robot design with significant potential for future advancements and practical applications while highlighting the trade-offs that designers should consider when adopting this methodology.**

I. Introduction

The Delta robot, introduced by Clavel in the 1980s [1], is one of the most widely studied and utilized parallel manipulators. The robot comprises three actuators on its base, which drive three parallel arms connected to an end-effector platform. The kinematic chains constrain the platform's motion to three translational degrees of freedom. The Delta robot is renowned for its light structure, high speed, and accuracy, making it ideal for packaging and pick-and-place operations [2]. Its versatile and adaptable architecture has led to its continued use in various novel applications across multiple fields.

A. Parmiggiani, E. Ottonello are with the Manufacturing and Design Facility, Centre for Robotics and Intelligent Systems (CRIS), Fondazione Istituto Italiano di Tecnologia (IIT) Via S. Quirico 19/D, 16163 Genova, Italy

E. Ottonello is with DIBRIS, University of Genova, Via all'Opera Pia 15/A, Genova, Italy

S.M. Kargar, M. Baggetta, G. Berselli are with the Department of Mechanical, Energy, Management and Transportation Engineering (DIME), University of Genova, Via all'Opera Pia 15/A, 16145 Genova, Italy

G. Hao is with the School of Engineering and Architecture-Electrical and Electronic Engineering, University College Cork Electrical Building 1.06, College Road, Cork, Ireland

G. Berselli is with the Advanced Robotics Department (ADVR), Fondazione Istituto Italiano di Tecnologia (IIT), Via S. Quirico 19/D, 16163 Genova, Italy

A few recent examples can be found in the work of Tran et al. [3], who equipped a Delta robot with an image processor to classify products and rapidly pick and drop them in a classification box, or in the work of Xiao et al. [4] that used a Delta robot in a robot-assisted retinal surgery system. Okunevic et al. [5] developed the DeltaCharger, a system based on Delta kinematics that can precisely position a set of electrodes to transfer energy between two robots. Hirano et al. [6] built a Delta robot driven by pneumatic artificial muscles. According to the authors, this device could be a rehabilitation and VR/AR haptic device.

It is interesting to note that compliant mechanisms are also utilized in some implementations. Compliant mechanisms, that replace joints with compliant elements such as flexure hinges or elastic bearings, have been extensively studied over the past two decades. Howell's [7], [8] and Lobontiu's [9] books offer comprehensive overviews of compliant mechanisms, including design approaches, guidelines, and examples of their applications.

For what concerns robot mechanisms, significant ranges of motion are generally necessary, and this can be challenging to achieve using compliant mechanisms because large ranges of motion require large joint strains, which, in turn, adversely affect durability and robustness. Therefore, it is important to consider the possible solutions that have been presented in the literature to tackle this issue.

Among the earliest compliant parallel robots is the work of Raatz et al. [10], which introduced a macro parallel robot that replaces conventional bearings with pseudo-elastic flexure hinges. The robot consisted of a spatial parallel structure with three translational degrees of freedom and driven by three linear direct-drive actuators. The symmetrical structure and optimized design of flexure hinges make it very stiff, and the experimental repeatability is below $0.3[\mu m]$.

The work by Correa et al. [11] is interesting as it presents one of the first comprehensive implementations of compliant joints for parallel robots, fabricated via the printed circuit MEMS (PC-MEMS) [12] technique. More in detail, their work describes the use of 2-D manufacturing techniques such as sheet-metal operations and laser cutting to create a laminated Delta robot with prismatic actuation by bending the robot out of the plane to achieve its 3D shape. This process is simple and cost-effective, making it ideal for use in open-source hardware technologies for fabricating low-cost and complex electromechanical systems.

The same approach was later followed by McClintock et al. [13], which developed the milliDelta, also using the PC-MEMS technique but at the millimetre-scale. The authors demonstrated that the milliDelta system can achieve precise motion of the payload relative to the workspace.

More recently, the group by Mannam et al. at Carnegie Mellon University (CMU) [14] introduced a compliant delta manipulator using 3D-printing and soft materials. The parallelogram links of the delta robot design were optimized by varying twelve dimensional parameters and two different materials. The resulting mechanisms were evaluated for stiffness by displacing them and observing the resulting forces and rotation angles, with the best combinations resulting in near-delta behavior. The same approach was later employed in [15] for a 3D-printed, low-cost and compliant gripper with two centimeter-scaled 3-DOF delta robots actuated by using off-the-shelf linear actuators. The authors also introduced the DeltaZ robot [16], a low-cost, centimeter-scale, delta-style robot which is affordable, easy to assemble and maintain.

While the work of Correa et al., McClintock et al. and Mannam et al. are noteworthy, their focus was primarily on the small scale, and only a few larger scale implementations have been reported to date. As such, the fabrication of compliant robots remains an open question.

In this context, we will focus on additive manufacturing (AM) as a potential solution. AM offers significant design freedom and cost-effectiveness, making it an invaluable tool for creating compliant joints that are difficult or impossible to manufacture with traditional methods. However, the implementation of compliant mechanisms using AM poses unique challenges related to the nature of the process.

For instance, Fowler et al. presented an evolution of the "butterfly-hinge" design by Henein et al. [17], which was fabricated using AM in titanium [18]. Merriam et al. developed a monolithic 2DOF pointing mechanism [19] for space applications, while Kiener et al. presented the construction of a flex-type pivot with interlocked flexure blades [20] and a compliant rotation reduction mechanism. In addition to utilizing metal components, AM can also facilitate the fabrication of compliant joints with plastic materials, that have the advantageous capability of accommodating larger strains, thereby enabling larger displacements than metals. For example, Sharkey et al. [21] presented a monolithic 3D-printed flexure translation stage, fabricated using material extrusion, that forms the key element of an open-source miniature microscope. Baggetta et al. [22] employed the same technology to realize a variable stiffness actuator to be used in humanoid robotics. Similarly, Almeida et al. [23] presented a 3D-printed flexure-based robotic microtweezers device for precision manipulation that was obtained using powder bed fusion, whereas a monolithic two-fingered push-latch gripper has been recently presented in [24]. These examples demonstrate the versatility of AM in the design and fabrication of compliant joints, and its potential to create large displacement joints for various applications, including aerospace, medical and robotic.

Additive manufacturing offers designers the freedom to create non-assembly mechanisms [25] i.e. mechanisms that do not necessitate any assembly procedures. These mechanisms are distinctive in that they can be utilized immediately after manufacturing. The adoption of non-assembly mechanisms presents several benefits, including time and cost savings due to the elimination of assembly operations, fewer tight tolerances to abide by, functional integration, and the absence of components, bearings or fasteners, resulting in weight reduction. Such advantages make non-assembly mechanisms a practical choice for specific applications that prioritise time and cost efficiency.

Finally, this study draws inspiration from the works of Bruyas et al. [26], Rommers et al. [27], and Naves et al. [28]. The work of Bruyas et al. [26] is significant for being one of the earliest to present a 2DOF mechanism fabricated monolithically using multi-material printers. In 2021, Rommers et al. [27] introduced the "Tetra1 " and "Tetra 2" designs for large range of motion spherical joints, with the latter being particularly well-suited for additive manufacturing and used as one of the key building blocks of the current work. Additionally, Naves et al. [28] recently demonstrated the feasibility of high-precision parallel robots with large workspaces, utilising only compliant joints. Some of the key concepts from these works were adapted and integrated into the present work.

To summarise, the contributions of the current work lie in four main differences between the presented mechanism and existing Delta robot implementations in the literature:

1) previous implementations mainly focused on flexure hinges, whereas the current design heavily relies on the "Tetra 2" spherical joint to achieve higher mobility;
2) the presented mechanism is larger, resulting in a larger workspace, which in turn complicates manufacturing and the achievement of high precision;
3) all other compliant delta implementations (with the notable exception of [11]) only focused on the final articulated quadrilaterals, whereas a full robot was developed in this work;
4) it is completely monolithic and is fabricated in a single manufacturing step.

The relevance of monolithic mechanisms lies in the fact that they do not require additional components such as bearings to function. Hence, they can be built and deployed on-site even in remote geographical locations (e.g. deserts, deep jungles, space, etc). Another advantage of this development approach is that it is resilient to supply chain disruptions where off-the-shelf components are unavailable, as recently witnessed because of pandemics and extreme weather events. From a wider perspective, a further element of significance of this study lies in the fact that AM expedites the development cycles of robots, which can be advantageous for various purposes. For instance, this approach could facilitate the acceleration of prototype development and deployment, and enable experimentation with new robot kinematics.

Furthermore, the use of compliant mechanisms is particularly advantageous for applications where joint lubrication is a concern, such as in extreme environments (e.g. space, deep sea, etc.) or medical applications.

The practical implementation of this approach, as presented in this work, sheds light on the trade-offs that designers must

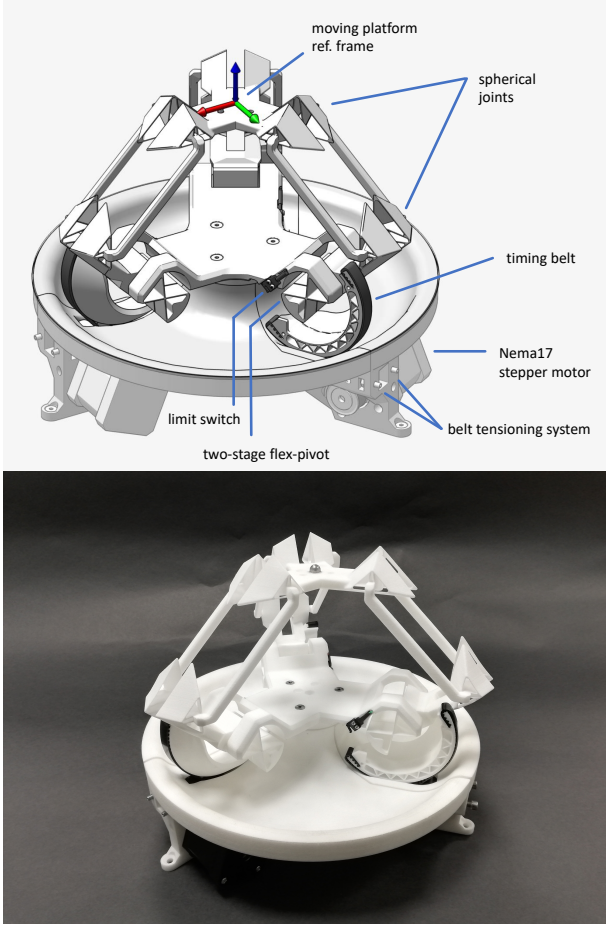


Fig. 1. CAD view and photograph of the DeltaFlex

confront should they choose to adopt this methodology.

II. System Design and Implementation

Compliant joints typically exhibit restricted ranges of motion, posing a considerable challenge in achieving substantial workspaces for robots. Parallel architectures are, however, particularly well-suited for implementations with flexible joints (as the work of Naves et al. [28] demonstrates), given that the required range of motion for individual joints is often lesser than that required for serial architectures. In light of the aforementioned considerations, the Delta architecture was selected for this study. The system implementation is represented in Fig.1 which shows an overall view of the DeltaFlex and its main parts.

Notwithstanding the parallel architecture, achieving extensive ranges of motion for the joints remained challenging. To address this issue, a two-stage cart-wheel flex-pivot was utilized for implementing the rotational joint of each arm in the base. For the same reason, the four spherical joints of each arm were constructed with a design drawing inspiration from the "Tetra 2" joint developed by Rommers et al. [27], albeit with some slight modifications to enhance the range of motion and prevent self-collisions (see [29] for further details). Fig.2 represents the joint developed by Rommers et al. and the spherical joint adopted for the DeltaFlex.

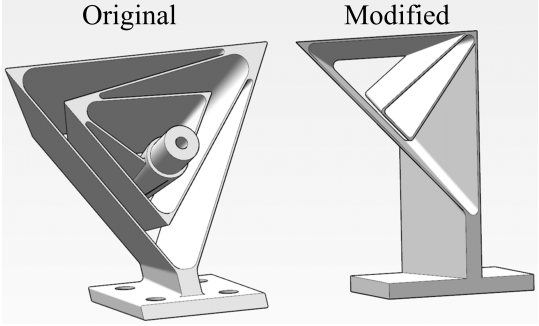


Fig. 2. Comparison between the spherical joint adopted in this work and the original design by Rommers et al. [27]

Moreover, a Design for Additive Manufacturing (DfAM) strategy was adopted for the entire robot. In this study, powder bed fusion was chosen as the manufacturing technology due to its cost-effectiveness and because it does not require the addition of support structures. However, owing to the DfAM methodology employed, the geometry obtained is also well-suited for fused material extrusion printers, which are more prevalent.

To adapt the design for material extrusion, it necessitates being divided into three distinct parts as represented in Fig.3. The resulting mechanism, consequently, loses its monolithic nature but this change does not imply a substantial deviation from the fundamental approach "philosophy" as it remains true that the mating interfaces do not demand tight coupling tolerances.

Specifically, all the flexures in each arm were designed to develop orthogonally to a shared orientation. Selecting this direction as the build direction maximises the mechanical strength of each flexure. "Tetra 2" spherical joints were developed with an inclination of 45°. This allowed avoiding the addition of supports hence the degradation of surface quality in this critical region. To reduce the need for support structures, horizontal geometric features were gradually extended from the side surfaces at an inclination exceeding 45°, rendering them self-supporting. Additionally, features exhibiting over-

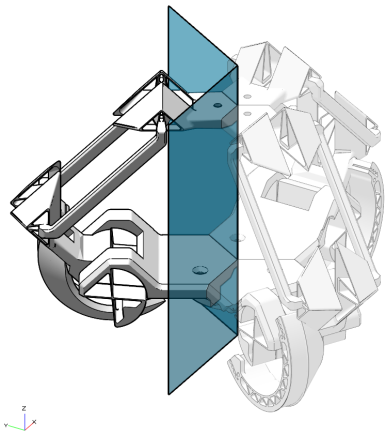


Fig. 3. Mechanism sub-division for compatibility with material extrusion AM.

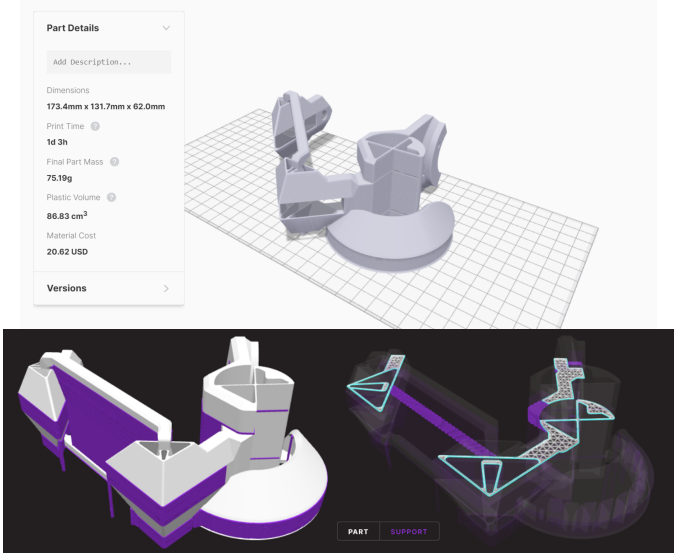


Fig. 4. Build strategy. The figure shows the divided part overall view (top) and sliced view (bottom) in the Markforged eiger slicing software. Notably, the bottom-right detailed layer view, demonstrates that the flexures are support-free, a crucial aspect of the design.

hangs were eliminated wherever feasible. The build strategy of the modified part, compatible with material extrusion AM, is represented in Fig.4

The mechanism implementation described in the current work was manufactured via powder bed fusion on a 3D Systems ProX SLS 6100 machine with DuraForm as construction material. DuraForm PA is a durable polyammide 12 thermoplastic (a.k.a. Nylon) with good structural properties which also exhibits close to isotropic behaviour once manufactured. Furthermore the high value of deformation at break (14%) makes this material particularly suitable for the construction of compliant mechanisms. All flexures were designed with a thickness of 0.7[mm], which was found to be the lowest thickness value that could be reliably manufactured on the ProX SLS 6100.

The actuation of each arm was achieved through the use Nema17 stepper motors, because of their high holding torque and ease of control. The motors used for this device had a step angle of 1.8°, a holding torque of 0.59[Nm] and an input voltage of 2.80[V]. The driving motors were connected to a driven pulley integrated directly on the first link of each arm with a timing belt, thus achieving a transmission ratio of 3.8:1. The belt tensioning system (represented with its components in detail in Fig.5) was integrated directly in the support structure of the device.

The motors were controlled with an Arduino UNO WIFI rev.2 (ATmega4809 8-bit microcontroller) and a 3-Axis CNC/Stepper Motor Shield that controlled the motors through A4988 stepper drivers. An Omron D2MQ-4L-105-1 limit-switch was installed on each axis to achieve the initial homing of the device.

To facilitate the replication of this study, all models and materials have been made accessible on a GitHub repository[1].

III. Experiments

The quantitative evaluation of the DeltaFlex's performance focused on two primary aspects, namely stiffness and precision. The assessment of stiffness involved measuring the device's ability to endure applied loads, a critical factor in ensuring motion precision under diverse operating conditions. Although conventional robots with rigid links and bearings are generally not affected by this issue, it assumes greater significance in the case of robots with compliant joints. The stiffness assessment was carried out using two distinct tests. The first test determined the mechanism's translation stiffness under normal operating conditions, where the moving platform translated parallel to the fixed base. The second test aimed to evaluate the mechanism's ability to resist offset loads that could lead to the tilting of the moving platform, thereby adversely affecting the device's ability to move solely in the x, y, and z directions, without unwanted rotations. Finally, the third test aimed at quantifying the precision of the mechanism through the assessment of its repeatability.

A. Translation stiffness test

The stiffness of the device was characterised with a *Zwick-Roell Z050* tensile/compression testing machine, equipped with a load cell rated for 50[kN] full-scale load (with Class 1 accuracy in the ISO 7500-1 standard). During the tests, the base of the robot was kept fixed, while the end-effector was locked to the moving traverse. The motion of the traverse loaded to the robot which then deformed; while doing so, forces and displacements were recorded. The speed of the moving traverse was 30 mm/min. Two different configurations were tested: in the first, the robot was installed with the moving platform perpendicular to the direction of movement of the moving traverse, while in the second configuration,

[1]https://github.com/made-iit/public/deltaflex

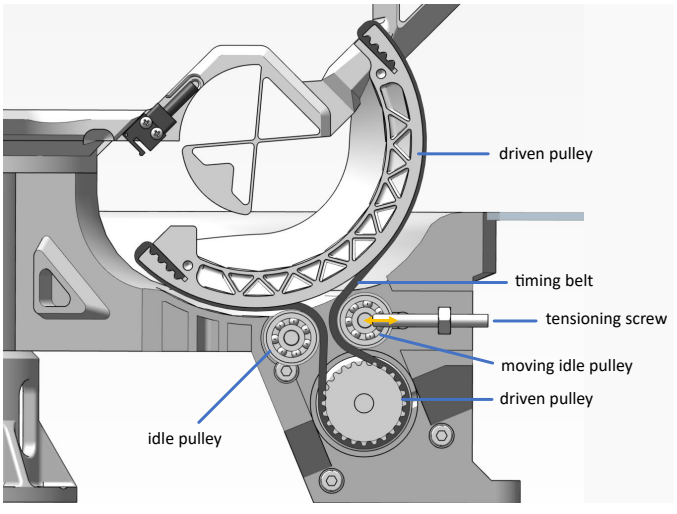


Fig. 5. Belt tensioning mechanism

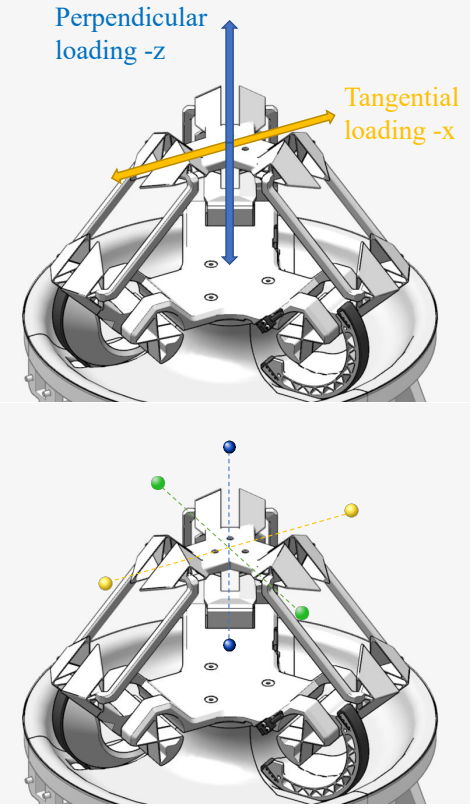


Fig. 6. Different load configurations and reference configurations. The figure represents the perpendicular and tangential loading directions (left), as well as the end-effector positions corresponding to the six test configurations. The colour coding (x in yellow, y in green and z in blue) is the same used in Fig.11.

the moving platform was kept parallel to the direction of movement of the moving traverse. Fig. 6 represents these configurations. Starting from the home configuration, both loading conditions were applied bidirectionally by performing both descending and ascending movements of the moving traverse. This allowed evaluating the behaviour of the robot in opposite directions. To obtain statistical data, the test was replicated five times in all conditions and the outcomes were averaged.

B. *Offset loading test*

The second stiffness evaluation was conducted in the following manner. The end effector was repositioned into six reference configurations, each in proximity to the robot's workspace boundaries. Subsequently, the input joints were secured in place using a custom-designed fixture to eliminate the effects of the belt transmission on the experimental results. The Cartesian coordinates of the six reference configurations are listed in table I. Once the input joints were then locked, the end effector's position and orientation were measured. Calibrated weights of 50[g], 100[g], 150[g] and 200[g] were subsequently applied onto the mobile platform in an offset position having a distance of 200[mm] from the end effector's centre. This is equivalent to the application of a wrench with components $[0, 0, -9.81 \cdot W, 0, 0.2 \cdot 9.81 \cdot W, 0]$ to the end effector (i.e. negative force in the z direction and positive torque in the y direction), where W corresponds to the weight of the calibrated weight utilized. To provide an indication of the approximate order of magnitude, the maximum applied force was -1.96[N] and the maximum applied torque was 0.39[Nm]. For every load condition the end effector's position and orientation were measured three times. Measurements were made with a Shining 3D Einscan XH 3D scanner. The laser modality was employed in conjunction with marker-based tracking to enhance measurement precision. In this condition the scanner has an accuracy of 0.04[mm].

Upon measuring all positions and orientations, the Euler angles denoting the three-dimensional rotations of the end effector were extracted. This was achieved by fitting coordinate system features to the obtained scans. It is important to note that this fitting procedure can yield errors in the order of 0.5°.

The configuration of the moving platform was measured before and after applying the loads. This approach enabled the distinction between the platform's tilting due to its displacement from the home configuration and the tilting caused by the applied loads. The utilisation of this method was crucial, as it would not have been feasible to perform using a material testing machine.

C. *Repeatability test*

Finally, the third test was performed to assess the repeatability of the robot. This performance indicator is critical for applications that require high precision and accuracy (e.g. the manufacturing industry). To do so, the robot's end-effector was moved to six different reference configurations close to the limits of the robot's workspace for twenty repetitions. In each repetition, the final position of the end-effector was measured with a *TESA 01811001 SwissTast* micrometric dial gauge (range: 0.2[mm], resolution: 0.002[mm], measuring force: 0.15[N]). To attain reproducibility of the test, the probe made contact with an 8[mm] diameter calibrated, hardened stainless-steel sphere. The experimental setup is shown in Fig.7.

IV. Results

The results of the stiffness test are represented in Fig.8.(a) for the case of loading directed perpendicularly to the end-effector, and in Fig.8.(b) for the case of transversal loading. In both cases the ascending load path (robot subject to traction force) and the descending load path (robot subject to compression force) are represented in green and blue respectively. The curves represent the average of all the experimental runs while the the shaded bands above and below the curve represent

TABLE I
Cartesian coordinates (in millimetres) of the six reference configurations used for the tests

x+	[38, 0, 0]
x-	[-38, 0, 0]
y+	[0, 38, 0]
y-	[0, -38, 0]
z+	[0, 0, 42]
z-	[0, 0, -42]

the standard deviation of the experimental data. Arrows were superimposed to the plots to indicate the sections of the curves that correspond to the increasing load and decreasing load phases. A linear fit of the force-displacement curve in the perpendicular loading case yields a stiffness value of 0.41[N/mm]; for the tangential loading case the computed stiffness is 0.19[N/mm].

A first observation is that in each condition the loading and unloading of the robot do not follow the exact same force-displacement trajectory; this gives rise to a narrow hysteresis loop. This is somewhat surprising considering there are no bearings with relatively moving parts and all robot motion is due to the flexures' deflection which should be nearly frictionless. Subsequent material testing was undertaken with the aim of quantifying the extent of hysteresis within the material and results substantiated the significant presence of hysteresis behavior. Secondly, the force-displacement curve is not perfectly linear. This effect could be due to either the effect of large deformation or to non-linear material properties. Further testing will be required to ascertain what phenomenon causes this effect.

Despite these drawbacks, the overall value of stiffness of the robot is relatively low; this means the DeltaFlex achieves a significant range of motion while opposing a relatively low resistance to movement, (which is a highly desirable characteristic for compliant mechanisms).

The results of the second stiffness evaluation are presented in Fig.9 and Fig.10, and allow several noteworthy observations. Figure 9 represents the translation errors of the platform in the six reference configurations when no loads were applied. Although error values were typically below 3[mm], some exceed this threshold (consistently with previous literature, e.g. [14], [15]). As such, open loop control would not constitute a viable solution for a mechanism of this kind, and closed position feedback would be necessary for precise end-effector position control. This, however, introduces the challenge of accurately measuring the end-effector's pose. Figure 10 represents the effects of offset loads on the end-effector's tilt. Primarily, for configurations where the end effector underwent lateral translation in the y direction (i.e., the "y+" and the "y-"

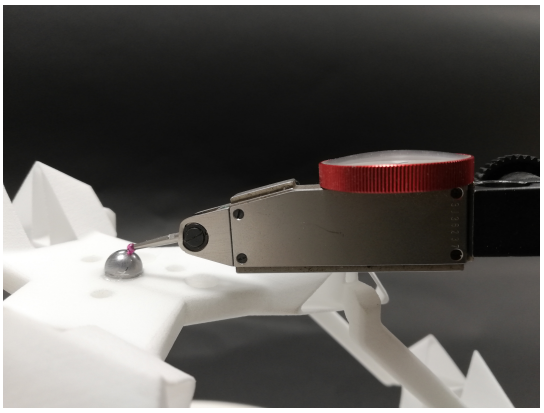


Fig. 7. Repeatability test setup. The photograph represents the setup with the micrometric dial gauge and the calibrated steel sphere that was used for the tests.

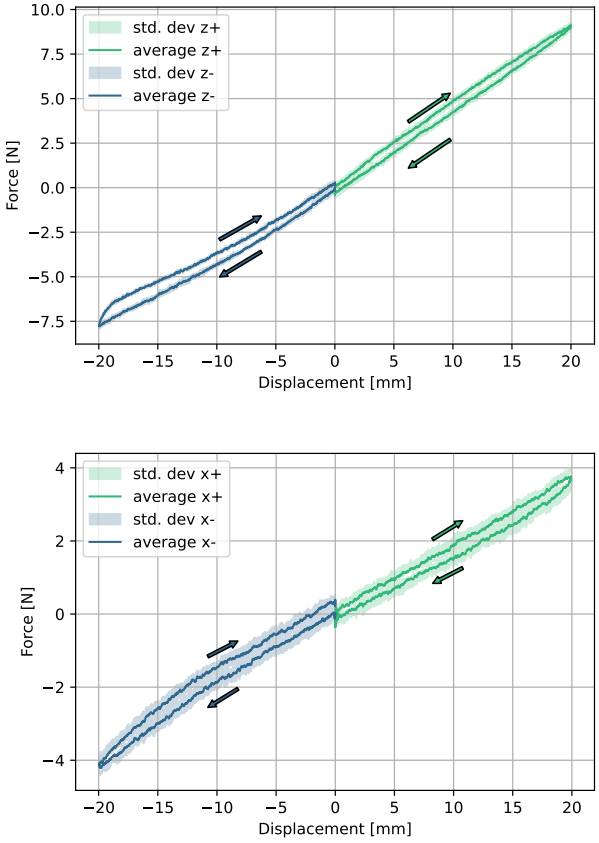


Fig. 8. Experimental results of the stiffness tests. The figure represents the force-displacement curve for the case of perpendicular loading (top) and the force-displacement curve for the case of tangential loading (bottom).

conditions), a relevant orientation drift, between +8° and -12°, was measured. Conditions "x+" and "x-", show similar drifts but in this case bounded between +7° and -8°. These results thus indicate that the motion of the mechanism within its workspace has an effect on the platform's tilting. In contrast, as expected, the influence of end-effector displacement and offset loads on rotations around the z-axis was found to be negligible (see the z Euler angle graph).

Figure 10 illustrates that a linear increase in the applied loads corresponds to a proportional increase in the platform tilt across all tested configurations. This effect is especially evident in the plot y Euler angle. Consequently, the mechanism can be deemed to exhibit linear behaviour within the tested range of forces. Notably, the employment of compliant joints resulted in orientation errors that exceed those that would have been encountered if a traditional design approach with conventional bearings had been adopted. This aspect should be thus taken into account while considering subsequent applications of the mechanism.

Nevertheless, after a comprehensive assessment of kinematic errors, the current design could prove useful for applications necessitating scanning or pointing motions.

The results of the repeatability test are shown in Fig.11. The plot shows how for the six chosen test configurations the

average position shift is less than 30[μm], indicating good repeatability.

V. DeltaFlex Virtual Prototyping

Structural and motion simulations are a powerful tool for verifying the experimental results of a robotic system. In this case, the aim is to simulate the DeltaFlex robot using RecurDyn, a flexible multibody dynamics software, to verify the experimental results for stiffness analysis, direct kinematics, and Euler angles. This computer-aided tool has been previously employed by the authors for the sizing and the subsequent shape-optimization of compliant joints and devices made therewith [30]. In addition, by modeling the robot in a virtual environment, its behaviour can be studied, the simulation results can be compared with the experimental data to make informed decisions in the design process, and the geometry of the compliant joints can be optimized.

To perform the simulation, the 3D model designed in PTC Creo was imported into RecurDyn, as it can be seen in Fig.12 and assigned the material properties for Nylon from RecurDyn's library. The links, base, and end-effector were treated as rigid bodies. The flexures were meshed using a minimum and maximum mesh size of 0.2 and 1.2, respectively, and a triangular mesh was chosen for the mesh type. To replicate the experiments, ±20[mm] displacement in both horizontal and vertical directions were defined with a point on curve (PTCV) joint. The reaction forces on the joint were measured for the input displacement to plot the force-displacement graphs for both cases, as shown in Fig.13. To determine the material Young's modulus for simulations, the results obtained from material hysteresis tests were utilised to replicate a tensile test within RecurDyn. Following this, optimisation techniques were applied to fine-tune the Young's modulus of the model, ensuring alignment with experimental data in terms of the output force-displacement curve. The simulation results confirmed the experimental findings, revealing a low stiffness in the robot's desired directions of motion. The force-displacement curve for the vertical loading case showed a slight non-linearity that could be attributed to the effect of large deformations. To verify the experimental findings on direct kinematics and Euler angles, another simulation was

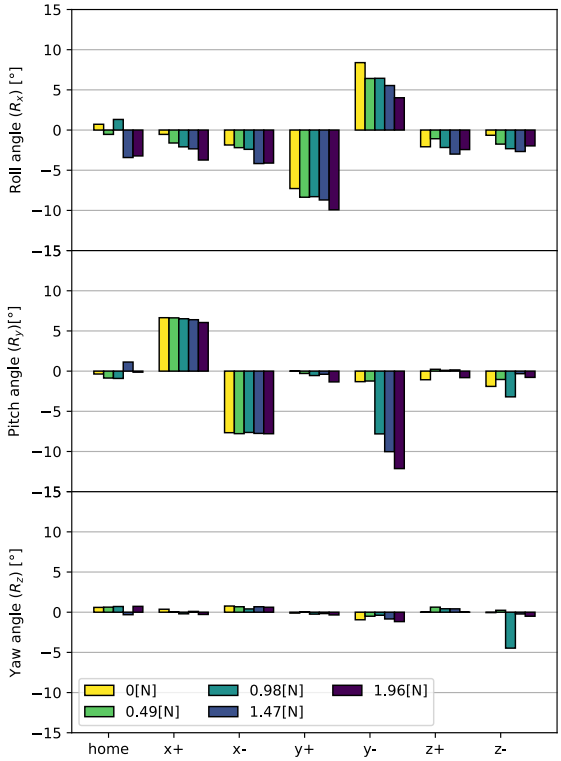


Fig. 10. Results of the stiffness tests under offset loads. The figure presents the roll, pitch and yaw angles measured in seven reference configurations for five increasing offset loads. The corresponding test configurations are labelled as in table I.

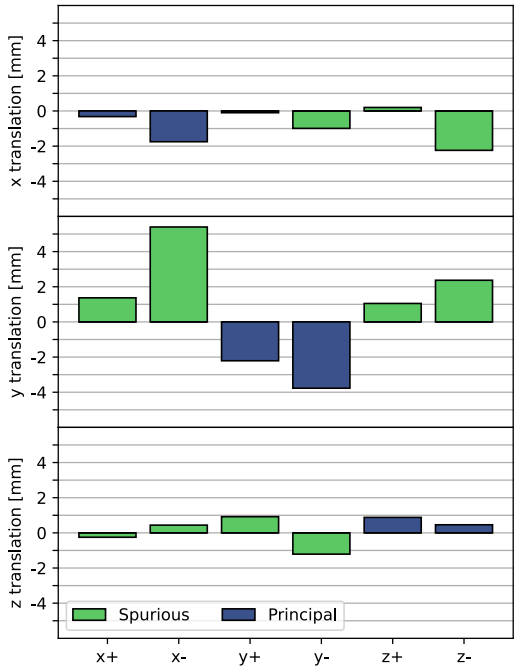


Fig. 9. End effector translation errors. The figure presents the end-effector's x, y, and z translation errors for the reference configurations. The errors along the principal directions are plotted in blue, whereas the errors in the spurious directions are plotted in green. The corresponding test configurations are labelled as in table I.

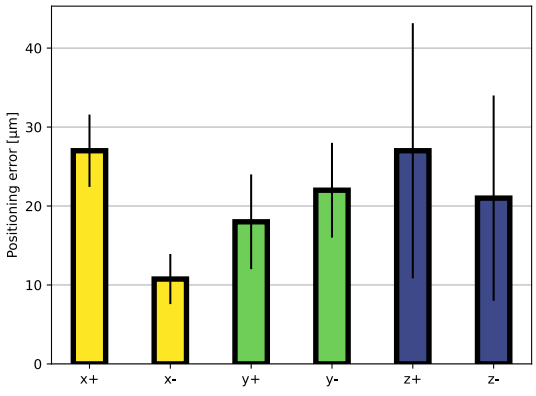


Fig. 11. Repeatability test results. The histograms represent the repeatability error and their standard deviations for the six reference test configurations of table I.

performed. The same input rotations used in the experiments were imported to the FEA model in RecurDyn. The output translations and Euler angles obtained from the simulations are compared to the experimental values in Fig.14. The graphs demonstrate good agreement between the numerical values obtained from the simulations and the experimental results. This observation indicates that the simulation model, despite its approximations, accurately captures the overall behaviour of the mechanism, even accounting for spurious roto-translations.

VI. Kinematic errors assessment

A further advantage of the FEM hybrid model of the entire compliant mechanism lies in its capacity to elucidate the individual contributions of various joint errors to the overall kinematic error. To investigate this aspect a subsequent analysis was conducted to evaluate the impact of parasitic motion originating from the different flexures. More in detail, three different models were developed in the RecurDyn environment and compared, namely:

- Model 1: *Fully Rigid Model*, where all joints are represented as rigid bodies, with revolute and spherical joints.
- Model 2: A model where the three base cross-axis flexures are treated as rigid and replaced with revolute joints, while the spherical joints are flexible *Tetra 2* joints.
- Model 3: A model in which the compliant *Tetra 2* joints are replaced with rigid spherical joints, while the cross-axis flexures remain flexible.

To evaluate the accuracy of the models, their simulated motions were compared to a "baseline" model computed using the analytical inverse kinematics. As an example, a helical trajectory involving motion in all three translational directions of the Delta robot's end-effector was applied. For each configuration, the input joints rotations (i.e. the "actuators'" rotations) were recorded. These rotations were then applied as inputs in the three simulation models, and the corresponding output trajectories at the end-effector were recorded. The resulting trajectories are shown in Fig. 15. To quantify the error or deviation between these trajectories and the reference trajectory, the Euclidean distance between corresponding points of the trajectories was calculated and plotted in Fig. 16. This figure provides insight into how much the trajectories deviate from the reference one.

As can be seen, the "Fully Rigid Model" (i.e., the one with ideal revolute and spherical joints) exactly replicates the analytically computed trajectory. The trajectory of Model 3 closely follows the baseline trajectory as well, and the Euclidean distance error is also low, indicating that the cross-axis flexures exhibit a high degree of precision, closely resembling the results of the rigid model. Finally, the model containing flexible "Tetra 2" joints (Model 2) exhibits the highest deviations from the original trajectory, thus displaying the highest errors. This highlights the fact that the errors plotted in Fig.14 are mainly caused by the "Tetra 2" joints not behaving exactly like spherical joints. This underscores an important design trade-off: the use of "Tetra 2" joints is well-suited for additive manufacturing but affects the mechanism's

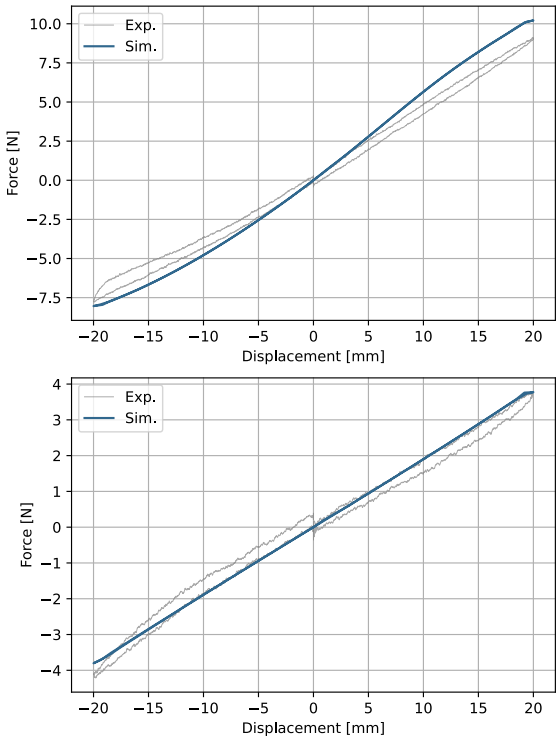


Fig. 13. Results of the stiffness simulations in RecurDyn. The figure represents the force-displacement curve for the case of perpendicular loading (top) and tangential loading (bottom). The results obtained from the RecurDyn simulations ("Sim." label) were superimposed to the averaged experimental data (grey line, "Exp." label; see Fig.8), to illustrate their degree of concordance.

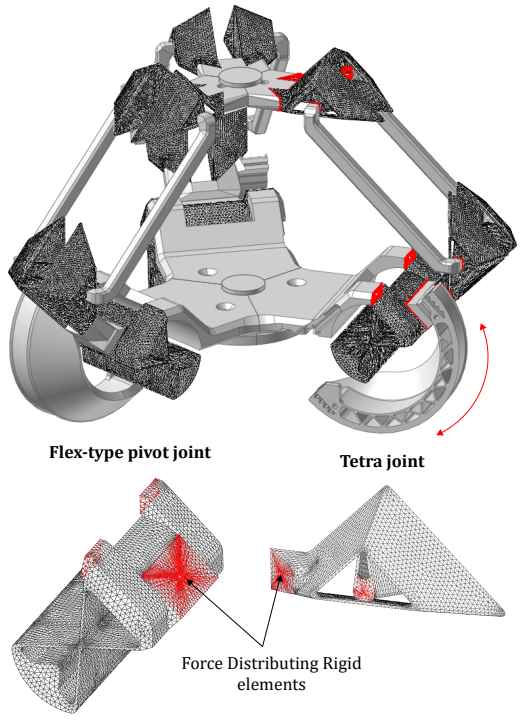


Fig. 12. Hybrid model in RecurDyn. The figure shows the 3D model developed within the Recurdyn environment that was used for the simulations. The meshed regions correspond to the flexible parts of the model, whilst the grey parts represent the indeformable solid bodies.

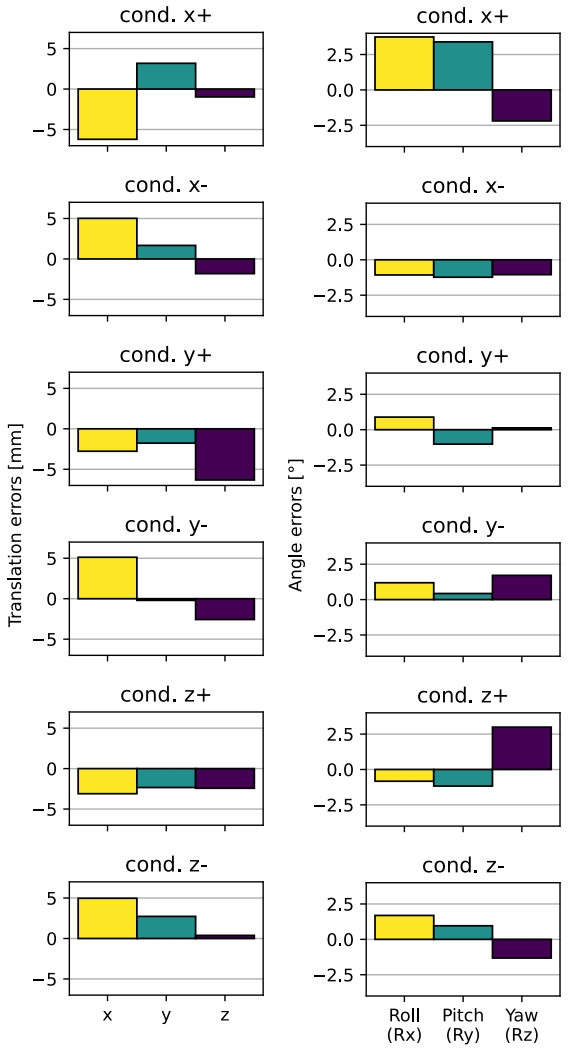


Fig. 14. Platform translation and rotation errors. The figure presents a comparison of the platform positioning errors retrieved from the simulations and the ones experimentally measured, in relation to six test configurations (as in Tab. 1). For instance, the upper left and right plots respectively provide translation and rotation errors (simulation vs experiments) concerning the x+ configuration. I.

overall motion precision.

VII. Discussion

The practical implementation of this work revealed several aspects whose knowledge could be helpful for further research and for other researchers.

1) As observed in the experimental investigation, the DeltaFlex exhibited substantial sensitivity to tilting moments applied to the end effector, which had a considerable impact on its capability to perform pure translations. It is thus important to consider the influence of spurious forces and moments on parasitic motion during the design phase and devise appropriate measures to counteract these. Our study represents one of the initial attempts to experimentally investigate this aspect, and we recommend incorporating this evaluation in forthcoming research.

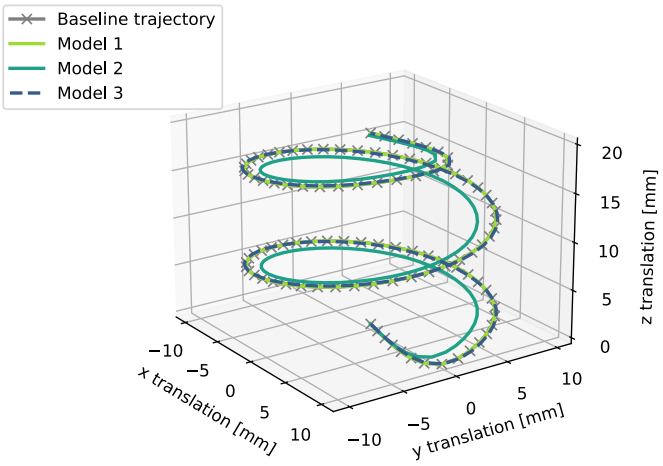


Fig. 15. End effector trajectories of the four simulation models. The figure provides an overview of the three dimensional trajectories of the three different simulation models.

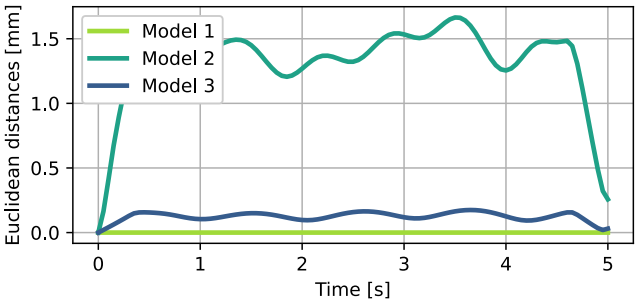


Fig. 16. Euclidean distance errors. The figure shows the Euclidean distance errors in millimetres for the three different models with respect to the baseline trajectory.

2) Another challenge we faced was the difficulty in measuring the mechanical properties of the DeltaFlex. Our initial attempt to utilise a high-precision coordinate measuring machine (CMM) to obtain measurements failed because the force needed to trigger the probe proved to be excessively high, leading to undesired movement in the mechanism. We thus opted for an optical instrument (3D scanner) to tackle this issue. This underlines the necessity for alternative contact-less techniques to measure the mechanical properties of compliant robots.
3) Upon comparing the test and simulation data, we observed a discrepancy in the material properties, which we resolved by tuning the material model used in the simulations. Researchers conducting similar tests should exercise caution and refrain from assuming perfect accuracy of the information reported in material datasheets.

VIII. Conclusions and Future Developments

The conducted tests provide an evaluation of the DeltaFlex's key characteristics, highlighting its low stiffness that results in reduced resistance to motion and high repeatability. These findings suggest that the DeltaFlex has the potential to be used

in a variety of applications where precision and accuracy are of utmost importance. Additionally, the experimental outcomes revealed areas that have room for optimisation and improvement.

The current prototype utilised stepper motors for actuation. However, in subsequent versions, the actuation system could be improved by integrating low gear ratios and brushless DC (BLDC) motors. This modification would allow for torque control during interaction tasks, thereby enhancing the system's precision and versatility.

Future work will include a comprehensive examination of the flexures' fatigue life in relation to the applied loads and the number of loading cycles. Additionally, exploring alternative materials and fabrication methods, such as material extrusion, could further enhance the existing knowledge.

In conclusion, despite the minor setbacks mentioned above, we assert that the methodology presented in this study offers a valuable approach to robot design with many opportunities for future advancements and practical applications.

REFERENCES

[1] Clavel, R., 1987. Device for displacing and positioning an element in space, WIPO Patent WO1987003528A1.

[2] Staicu, S., 2019. *Dynamics of Parallel Robots*. Springer International Publishing.

[3] Do, T. V., City, H. C. M., Viet, N. Q., Nam, N. Q., Dat, P. N., Vinh, D. D., and Hung, T. V., 2021. "Design of delta robot using image processing for product sorting process". *2021 International Conference on System Science and Engineering (ICSSE)*, 8, pp. 210–214.

[4] Xiao, B., Alamdar, A., Song, K., Ebrahimi, A., Gehlbach, P., Taylor, R. H., and Iordachita, I., 2022. "Delta robot kinematic calibration for precise robot-assisted retinal surgery". *2022 International Symposium on Medical Robotics, ISMR 2022*.

[5] Okunevich, I., Trinitatova, D., Kopanev, P., and Tsetserukou, D., 2021. "Deltacharger: Charging robot with inverted delta mechanism and cnn-driven high fidelity tactile perception for precise 3d positioning". *IEEE Robotics and Automation Letters,* **6**, 10, pp. 7604–7610.

[6] Hirano, J., Tanaka, D., Watanabe, T., and Nakamura, T., 2014. "Development of delta robot driven by pneumatic artificial muscles". *2014 IEEE/ASME International Conference on Advanced Intelligent Mechatronics*, 7, pp. 1400–1405.

[7] Howell, L. L., 2001. *Compliant Mechanisms*. John Wiley and Sons.

[8] Howell, L. L., Magleby, S. P., and Olsen, B. M., 2013. *Handbook of Compliant Mechanisms*. John Wiley and Sons.

[9] Lobontiu, N., 2001. *Compliant Mechanisms : Design of Flexure Hinges*. CRC Press, 11.

[10] Raatz, A., Wrege, J., Soetebier, S., and Hesselbach, J., 2004. "High precision compliant parallel robot with an optimized large workspace". In International Design Engineering Technical Conferences and Computers and Information in Engineering Conference (IDETC-CIE), pp. 1007–1014.

[11] Correa, J. E., Toombs, J., Toombs, N., and Ferreira, P. M., 2016. "Laminated micro-machine: Design and fabrication of a flexure-based delta robot". *Journal of Manufacturing Processes,* **24**, pp. 370–375.

[12] Sreetharan, P. S., Whitney, J. P., Strauss, M. D., and Wood, R. J., 2012. "Monolithic fabrication of millimeter-scale machines". *Journal of Micromechanics and Microengineering,* **22**, 4, p. 055027.

[13] Mcclintock, H., Fatma, Temel, Z., Doshi, N., Koh, J.-S., and Wood, R. J., 2018. "The millidelta: A high-bandwidth, high-precision, millimeter-scale delta robot". *Science Robotics,* **3**, 1.

[14] Mannam, P., Kroemer, O., and Temel, F., 2021. "Characterization of compliant parallelogram links for 3d-printed delta manipulators". In International Symposium on Experimental Robotics, pp. 75–84.

[15] Mannam, P., Rudich, A., Zhang, K., Veloso, M. M., Kroemer, O., and Temel, F. Z., 2021. "A low-cost compliant gripper using cooperative mini-delta robots for dexterous manipulation". In Robotics: Science and Systems XVII.

[16] Patil, S., Alvares, S. C., Mannam, P., Kroemer, O., and Temel, F. Z., 2022. "Deltaz: An accessible compliant delta robot manipulator for research and education". In IEEE/RSJ Int. Conf. on Intelligent Robots and Systems (IROS), pp. 13213–13219.

[17] Henein, S., Spanoudakis, P., Droz, S., Myklebust, L. I., and Onillon, E., 2003. "Flexure pivot for aerospace mechanisms". In 10th European Space Mechanisms and Tribology Symposium, pp. 285–288.

[18] Fowler, R. M., Maselli, A., Pluimers, P., Magleby, S. P., and Howell, L. L., 2014. "Flex-16: A large-displacement monolithic compliant rotational hinge". *Mechanism and Machine Theory,* **82**, 12, pp. 203–217.

[19] Merriam, E. G., Jones, J. E., Magleby, S. P., and Howell, L. L., 2013. "Monolithic 2 dof fully compliant space pointing mechanism". *Mechanical Sciences,* **4**, pp. 381–390.

[20] Kiener, L., Saudan, H., Cosandier, F., Perruchoud, G., and Spanoudakis, P., 2019. "Innovative concept of compliant mechanisms made by additive manufacturing". *MATEC Web of Conferences,* **304**, 1, p. 7002.

[21] Sharkey, J. P., Foo, D. C., Kabla, A., Baumberg, J. J., and Bowman, R. W., 2016. "A one-piece 3d printed flexure translation stage for open-source microscopy". *Review of Scientific Instruments,* **87**, 2, p. 025104.

[22] Baggetta, M., Berselli, G., Palli, G., and Melchiorri, C., 2022. "Design, modeling, and control of a variable stiffness elbow joint". *The International Journal of Advanced Manufacturing Technology,* **122**(11), Oct, pp. 4437–4451.

[23] Almeida, A., Andrews, G., Jaiswal, D., and Hoshino, K., 2019. "The actuation mechanism of 3d printed flexure-based robotic microtweezers". *Micromachines,* **10**, 1, p. 470.

[24] Ottonello, E., Baggetta, M., Berselli, G., and Parmiggiani, A., 2023. "Design and validation of a push-latch gripper made in additive manufacturing". *IEEE/ASME Transactions on Mechatronics,* **28**(4), pp. 2083–2091.

[25] Lussenburg, K., Sakes, A., and Breedveld, P., 2021. "Design of non-assembly mechanisms: A state-of-the-art review". *Additive Manufacturing,* **39**, p. 101846.

[26] Bruyas, A., Geiskopf, F., Meylheuc, L., and Renaud, P., 2014. "Combining multi-material rapid prototyping and pseudo-rigid body modeling for a new compliant mechanism". In Proc. IEEE Int. Conf. on Robotics and Automation (ICRA), pp. 3390–3396.

[27] Rommers, J., van der Wijk, V., and Herder, J. L., 2021. "A new type of spherical flexure joint based on tetrahedron elements". *Precision Engineering,* **71**, pp. 130–140.

[28] Naves, M., Nijenhuis, M., Seinhorst, B., Hakvoort, W., and Brouwer, D., 2021. "T-flex: A fully flexure-based large range of motion precision hexapod". *Precision Engineering,* **72**, pp. 912–928.

[29] Kargar, S. M., Parmiggiani, A., Baggetta, M., Ottonello, E., Hao, G., and Berselli, G., 2024. "Optimization of a tetrahedron compliant spherical joint via computer-aided-engineering tools". *International Journal of Advanced Manufacturing Technology*.

[30] Bilancia, P., and Berselli, G., 2021. "An overview of procedures and tools for designing nonstandard beam-based compliant mechanisms". *Computer-Aided Design,* **134**, p. 103001.

LIST OF FIGURES

1 CAD view and photograph of the DeltaFlex . . . 3

2 Comparison between the spherical joint adopted in this work and the original design by Rommers et al. [27] . . . 3

3 Mechanism sub-division for compatibility with material extrusion AM. . . . 3

4 Build strategy. The figure shows the divided part overall view (top) and sliced view (bottom) in the Markforged eiger slicing software. Notably, the bottom-right detailed layer view, demonstrates that the flexures are support-free, a crucial aspect of the design. . . . 4

5 Belt tensioning mechanism . . . 4

6 Different load configurations and reference configurations. The figure represents the perpendicular and tangential loading directions (left), as well as the end-effector positions corresponding to the six test configurations. The colour coding (x in yellow, y in green and z in blue) is the same used in Fig.11. . . . 5

7 Repeatability test setup. The photograph represents the setup with the micrometric dial gauge and the calibrated steel sphere that was used for the tests. . . . 6

8 Experimental results of the stiffness tests. The figure represents the force-displacement curve for the case of perpendicular loading (top) and the force-displacement curve for the case of tangential loading (bottom). . . . 6

9 End effector translation errors. The figure presents the end-effector's x, y, and z translation errors for the reference configurations. The errors along the principal directions are plotted in blue, whereas the errors in the spurious directions are plotted in green. The corresponding test configurations are labelled as in table I. . . . 7

10 Results of the stiffness tests under offset loads. The figure presents the roll, pitch and yaw angles measured in seven reference configurations for five increasing offset loads. The corresponding test configurations are labelled as in table I. . . . 7

11 Repeatability test results. The histograms represent the repeatability error and their standard deviations for the six reference test configurations of table I. . . . 7

12 Hybrid model in RecurDyn. The figure shows the 3D model developed within the Recurdyn environment that was used for the simulations. The meshed regions correspond to the flexible parts of the model, whilst the grey parts represent the indeformable solid bodies. . . . 8

13 Results of the stiffness simulations in RecurDyn. The figure represents the force-displacement curve for the case of perpendicular loading (top) and tangential loading (bottom). The results obtained from the RecurDyn simulations ("Sim." label) were superimposed to the averaged experimental data (grey line, "Exp." label; see Fig.8), to illustrate their degree of concordance. . . . 8

14 Platform translation and rotation errors. The figure presents a comparison of the platform positioning errors retrieved from the simulations and the ones experimentally measured, in relation to six test configurations (as in Tab. 1). For instance, the upper left and right plots respectively provide translation and rotation errors (simulation vs experiments) concerning the x+ configuration. I. . . 9

15 End effector trajectories of the four simulation models. The figure provides an overview of the three dimensional trajectories of the three different simulation models. . . . 9

16 Euclidean distance errors. The figure shows the Euclidean distance errors in millimetres for the three different models with respect to the baseline trajectory. . . . 9

LIST OF TABLES

I Cartesian coordinates (in millimetres) of the six reference configurations used for the tests 5